The Astrophysical Journal, 776:83 (8pp), 2013 October 20 doi:10.1088/0004-637X/776/2/83

REIONIZATION ON LARGE SCALES. III. PREDICTIONS FOR LOW-ℓ COSMIC MICROWAVE BACKGROUND POLARIZATION AND HIGH-ℓ KINETIC SUNYAEV–ZEL'DOVICH OBSERVABLES

N. Battaglia[1], A. Natarajan[1], H. Trac[1], R. Cen[2], and A. Loeb[3]
[1] McWilliams Center for Cosmology, Wean Hall, Carnegie Mellon University, 5000 Forbes Avenue, Pittsburgh PA 15213, USA
[2] Department of Astrophysical Sciences, Princeton University, Princeton, NJ 08544, USA
[3] Harvard-Smithsonian Center for Astrophysics, Cambridge, MA 02138, USA
Received 2012 November 13; accepted 2013 August 7; published 2013 October 1

ABSTRACT

We present new predictions for cosmic microwave background (CMB) temperature (on small angular scales) and polarization (on large angular scales) anisotropies induced during the epoch of reionization (EoR). Using a novel method calibrated from radiation-hydrodynamic simulations, we model the EoR in large volumes ($L \gtrsim 2\,\mathrm{Gpc}\,h^{-1}$). We find that the EoR contribution to the kinetic Sunyaev–Zel'dovich power spectrum (patchy kSZ) ranges between $\sim$0.6–2.8 $\mu\mathrm{K}^2$ at $\ell = 3000$ for the explored parameter space. For each model, the patchy kSZ power spectrum is calculated from three large $15^\circ \times 15^\circ$ maps for better numerical convergence. Decreasing the size of these maps biases the overall patchy kSZ power to higher values. We find that the amplitude of the patchy kSZ power spectrum at $\ell = 3000$ follows simple scalings of $D^{\mathrm{kSZ}}_{\ell=3000} \propto \bar{z}$ and $D^{\mathrm{kSZ}}_{\ell=3000} \propto \Delta_z^{0.51}$ for the mean redshift ($\bar{z}$) and duration (Δ_z) of reionization. Using the constraints on $\bar{z}$ from the *Wilkinson Microwave Anisotropy Probe* seven year results and the lower limit on Δ_z from EDGES, we find a lower limit of $\sim$0.4 $\mu\mathrm{K}^2$ at $\ell = 3000$. *Planck* will infer the mean redshift from the Thomson optical depth imprinted in the low-ℓ polarization power spectrum. Future measurements of the high-ℓ CMB power spectrum from the Atacama Cosmology Telescope and South Pole Telescope should detect the patchy kSZ signal if the cross correlation between the thermal SZ effect and the cosmic infrared background is constrained. We show that the combination of temperature and polarization measurements constrains both $\bar{z}$ and Δ_z. The patchy kSZ maps, power spectra templates, and the polarization power spectra will be publicly available.

Key words: cosmic background radiation – cosmology: theory – intergalactic medium – large-scale structure of universe – methods: numerical

Online-only material: color figures

1. INTRODUCTION

Free electrons in the intergalactic medium (IGM) scatter photons from the cosmic microwave background (CMB) radiation, creating secondary anisotropies that distort the primordial anisotropies. These free electrons are initially ionized from the neutral IGM by the first stars and galaxies during the epoch of reionization (EoR). Thus, information from the EoR is imprinted on the CMB in both temperature and polarization. The temperature fluctuations are affected by the kinetic Sunyaev–Zel'dovich (kSZ) effect, which is Doppler shifting of CMB photons from the bulk motions of free electrons with respect to the CMB rest frame (Sunyaev & Zeldovich 1980). The polarization signal on large angular scales is sensitive to the polarization rotation sourced by free electrons from the beginning of the EoR to the present (e.g., Bond & Efstathiou 1987; Hu & White 1997; Zaldarriaga 1997; Liu et al. 2001; Komatsu et al. 2011), which induces a curl-free polarization signal (E mode). These are the two leading-order effects. There are other smaller order effects, such as fluctuations in the optical depth (e.g., Dvorkin & Smith 2009; Su et al. 2011; Natarajan et al. 2013), that are not discussed.

Already, measurements from the opacity of the Lyα forest (Fan et al. 2006b), the redshifted 21 cm signal (Bowman & Rogers 2012) from the experiment EDGES,[4] and the large-scale polarization of the CMB (Larson et al. 2011) indicate that reionization was extended. Further model-dependent constraints on the EoR come from measurements of quasar proximity zones (e.g., Wyithe et al. 2005; Fan et al. 2006a), a null result for intergalactic damping wing absorption in a $z = 6.3$ gamma-ray burst spectrum (e.g., Totani et al. 2006; McQuinn et al. 2008), detections of damping wing absorption in the IGM from quasar spectra (e.g., Mesinger & Haiman 2004; Mesinger & Furlanetto 2008; Bolton et al. 2011), and Lyα emitter number densities and clustering measurements (e.g., Malhotra & Rhoads 2004; Haiman & Cen 2005). Using a semi-analytic model for reionization, the South Pole Telescope (SPT) placed an upper limit on the duration of reionization (Reichardt et al. 2012; Zahn et al. 2012) from their multi-frequency measurements of the high-ℓ power spectrum of CMB secondary anisotropies. New CMB measurements of temperature and polarization anisotropies from the *Planck* satellite, the POLARBEAR experiment, the Atacama Cosmology Telescope (ACT), ACT-pol (ACT with polarization), SPT, SPT-pol (SPT with polarization), and CMBpol (Zaldarriaga et al. 2008) have the potential to constrain the EoR from CMB measurements alone.

The amplitude of the EE power spectrum at $\ell \lesssim 20$ measures the optical depth to reionization, τ, with the most recent constraint being $\tau = 0.087 \pm 0.015$ corresponding to a mean reionization redshift of 10.5 ± 1.2 (68% confidence level; Larson et al. 2011). The commonly used Boltzmann integrator CAMB (Lewis et al. 2000) calculates the EE power spectrum using a parametric hyperbolic tangent function for the ionization history. There are modifications to CAMB (Mortonson & Hu 2008) that allow any ionization history as an input.

[4] http://www.haystack.mit.edu/ast/arrays/Edges

The fractional contributions to the kSZ from the EoR (e.g., Gruzinov & Hu 1998; Knox et al. 1998; Valageas et al. 2001; Santos et al. 2003; Zahn et al. 2005, 2012; McQuinn et al. 2005; Iliev et al. 2007; Jelić et al. 2010; Mesinger et al. 2011, 2012; hereafter we refer to this contribution as the patchy kSZ) are the largest on small angular scales compared to the primary and other secondary CMB anisotropies. There is an additional contribution to the kSZ power spectrum that comes from lower redshifts (Ostriker & Vishniac 1986; Jaffe & Kamionkowski 1998; Ma & Fry 2002; Zhang et al. 2004; Shaw et al. 2012; hereafter we refer to this contribution as the homogeneous kSZ). Many of the previous models for the patchy kSZ signal were calculated in small volumes ($\lesssim$1 Gpc h^{-1}) and do not capture the large-scale features of the patchy kSZ maps, which is required to accurately calculate the power spectrum.

This is the third paper (Paper III) in a series that explores observable from the EoR produced via our semi-analytical models of reionization that are statistically informed by simulations with radiative transfer and hydrodynamics. We introduce our model in Battaglia et al. (2013, hereafter Paper I), look at the impact of a patchy optical depth on CMB observables in Natarajan et al. (2013, hereafter Paper II), and explore the 21 cm signal in Paper IV (P. La Plante et al. 2013, in preparation).

We present in this paper predictions for CMB observables. These predictions are made in large volumes ($L = 2$ Gpc h^{-1}) and the importance of going to such large volumes is demonstrated throughout this work. The *EE* polarization power spectra, the kSZ power spectra, and the maps from this paper will be made publicly available. In Section 2, we summarize our fast semi-analytical model and the simulations that these observables are based on. In Section 3, we present results for the *EE* power spectrum and the kSZ power spectrum. We discuss prospects for future measurements and conclude in Section 5. We adopt the concordance cosmological parameters that are consistent with *Wilkinson Microwave Anisotropy Probe* (*WMAP*) seven year results (Larson et al. 2011): $\Omega_{\rm m} = 0.27$, $\Omega_\Lambda = 0.73$, $\Omega_{\rm b} = 0.045$, $h = 0.7$, $n_{\rm s} = 0.96$, and $\sigma_8 = 0.80$.

2. PARAMETRIC MODEL FOR REIONIZATION

In Paper I, we developed a semi-analytic model for reionization based upon results from RadHydro simulations (for more details, see Trac et al. 2008; Paper I). In the simulations, we construct a reionization redshift field, $z_{\rm RE}(\mathbf{x})$, that tracks the redshift at which each gas cell becomes 90% ionized. We define the following fluctuation fields for density,

$$\delta_{\rm m}(\mathbf{x}) \equiv \frac{\rho(\mathbf{x}) - \bar{\rho}}{\bar{\rho}}, \tag{1}$$

and the reionization redshift,

$$\delta_{\rm z}(\mathbf{x}) \equiv \frac{[1 + z_{\rm RE}(\mathbf{x})] - [1 + \bar{z}]}{1 + \bar{z}}, \tag{2}$$

where $\bar{\rho}$ is the mean matter density and $\bar{z}$ is the mean value for the $z_{\rm RE}(\mathbf{x})$ field, which is approximately equal to the redshift of 50% ionization. The fluctuations in both the $\delta_{\rm m}$ and $\delta_{\rm z}$ fields are highly correlated on scales $\gtrsim$1 Mpc h^{-1}. We calculate a simple scale-dependent linear bias that relates these two fields and we represent this bias with the simple parametric form

$$b_{\rm zm}(k) = \left[\frac{\langle\delta_{\rm z}(k)\delta_{\rm z}(k)\rangle}{\langle\delta_{\rm m}(k)\delta_{\rm m}(k)\rangle}\right]^{1/2} = \frac{b_{\rm o}}{(1 + k/k_{\rm o})^{\alpha}} \tag{3}$$

that contains three parameters $b_{\rm o}$, $k_{\rm o}$, and α. The value for $b_{\rm o}$ that we use is determined from analytical arguments in Barkana & Loeb (2004). The fiducial parameter values for $k_{\rm o} = 0.185$ Mpc h^{-1} and $\alpha = 0.564$ are found by fitting the bias calculated from the simulations. We explore the parameter space of our model by varying $k_{\rm o}$ and α. The effects these parameters have on the EoR are that increasing $k_{\rm o}$ lengthens the duration of reionization while increasing α shortens reionization (Paper I). Physically, a shorter reionization process tends to have larger ionization bubble sizes that percolate more quickly, which in turn correspond to more luminous ionizing sources.

We generate the overdensity fields, $\delta_{\rm m}$, using a particle–particle–particle-mesh ($\rm P^3M$) *N*-body code that evolves 2048^3 dark matter particles in a 2 Gpc h^{-1} box down to $z = 5.5$. One could use a density field generated from other methods, such as Lagrangian perturbation theory, but we found that the density field from *N*-body simulations was the best match to radiative transfer simulations. This overdensity field is then convolved with a filter consisting of three elements: (1) a cubical top-hat filter, $\Xi(k)$, which deconvolves the smoothing used to construct $\delta_{\rm m}$ from the simulation; (2) a Fourier transform of a real space top-hat filter $\Theta(k)$, which smoothes $\delta_{\rm m}$ to a resolution of 1 Mpc h^{-1}; and (3) the bias function from Equation (3). The assembled filter takes the form

$$W_{\rm z}(k) = \frac{b_{\rm zm}(k)\Theta(k)}{\Xi(k)} \tag{4}$$

and we convolve the density field at $\bar{z}$ with this filter. The newly constructed δ_z field is Fourier transformed back to real space and converted to the $z_{\rm RE}(\mathbf{x})$ field by Equation (2) with the same $\bar{z}$ as the density field. Here the value of $\bar{z}$ essentially sets the midpoint of reionization. We now have a complete ionization history for the density field used, which is then used to make ionization fields and kSZ maps. We define the duration of reionization as

$$\Delta_z \equiv z(x_i = 25\%) - z(x_i = 75\%), \tag{5}$$

where x_i is the ionization history. The small-scale physical processes at early and late times of reionization are difficult to capture in simulations and semi-analytic methods. Thus, we defined Δ_z to exclude these epochs. For a detailed parameter study of $\Delta_z(k_{\rm o}, \alpha)$, see Paper I.

3. RESULTS

We present our model predictions for the integrated optical depth, τ, the low-ℓ *EE*-mode polarization power spectrum, and the contribution to the patchy kSZ power spectrum. These predictions are compared to current and projected constraints, as well as previous work.

3.1. Optical Depth and EE Polarization Power Spectrum

The optical depth from an observer to the CMB is given by

$$\tau = \sigma_{\rm T} \int_0^{l_*} n_{\rm e}(l) dl, \tag{6}$$

where $\sigma_{\rm T}$ is the Thomson cross section, $dl = c\,dt$ is the proper distance along the line of sight, l_* is the distance to the surface of last scattering, and $n_{\rm e}(l)$ is the ionized electron number density at distance l. Constraints on τ from CMB temperature anisotropies alone are degenerate with the amplitude of primordial fluctuations. These constraints are

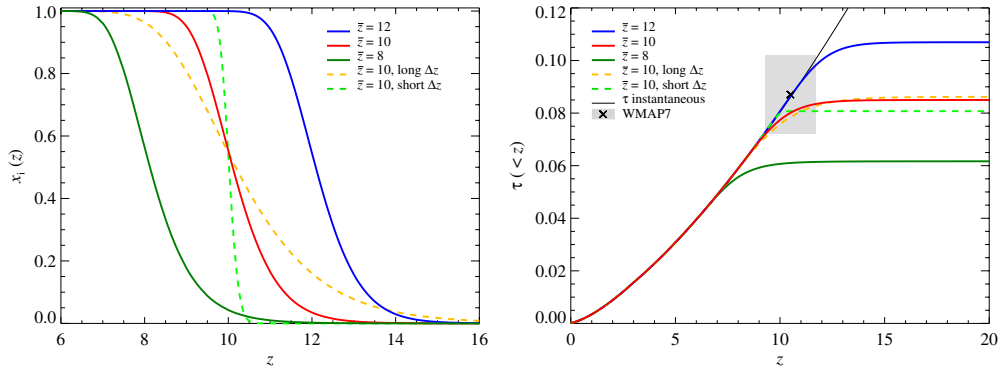

Figure 1. Left: the ionization fraction as a function of redshift, $x_i(z)$, for five models: our fiducial model at $\bar{z} = 8$, 10, and 12 (green, red, and blue, respectively) and two extreme models of long- (orange dashed) and short- (light green dashed) duration reionization at $\bar{z} = 10$. The $x_i(z)$ for the fiducial models have similar shapes and they are just shifted according to $\bar{z}$. Right: the corresponding optical depth, τ, for the same models as x_i. The values of τ are compared against the *WMAP* seven year constraint (light gray box; Larson et al. 2011) and their model-dependent constraint on the duration of reionization. Like the polarization power spectrum, a constraint on τ will differentiate between models with different $\bar{z}$, but cannot help differentiate between our models with large or small Δ_z.

(A color version of this figure is available in the online journal.)

significantly improved by the measurement of the low-ℓ *EE* polarization power spectrum. To first order, the amplitude of the low-ℓ *EE* power spectrum is proportional to τ^2. We calculate the large-scale *EE* polarization power spectrum using CAMB (Lewis et al. 2000) with the modifications by Mortonson & Hu (2008), which accepts general reionization histories, $x_i(z)$. Although novel, we did not include their principal component analysis (PCA) implementation.

The left panel of Figure 1 shows the results for $x_i(z)$ from our fiducial models at $\bar{z} = 8$, 10, and 12 and two extreme models for long- and short-duration reionization scenarios at $\bar{z} = 10$, while the right panel compares the *WMAP* seven year results to our results for the integrated τ. We show the corresponding *EE* polarization power spectra in Figure 2 and compare them to the *WMAP* seven year band power constraints (Larson et al. 2011). Comparing Figures 1 and 2 we find that the models with larger τ are consistent with having larger *EE* power at low ℓ. We find the fiducial parameters with $\bar{z} = 10$ agree with the *WMAP* constraint, and the 1σ confidence interval is bracketed by choices of $\bar{z} = 8$ and $\bar{z} = 12$. Our two extreme models of short- and long-duration reionization (hereafter small and large Δ_z) at fixed $\bar{z}$ differ from the fiducial model by a maximum 20% (cf. Figure 2). Figures 1 and 2 show that the current *WMAP* seven year data is unable to differentiate between these extreme models for reionization and given the projected error bars on the *EE* power spectrum (The Planck Collaboration 2006 for the 143 GHz channel and our fiducial model) neither will the upcoming observations from *Planck*. Thus, the current low-ℓ *EE* polarization power spectrum constraints are not sensitive to the duration of reionization. This conclusion is the same as previous work by Zahn et al. (2012); however, they come to this conclusion via a different semi-analytic model. Similarly, *WMAP* showed that only using the low-ℓ *EE* power spectrum constrains the mean redshift of reionization and is insensitive to the duration (e.g., Komatsu et al. 2011). There is no benefit when we include the low-ℓ *TE* cross spectrum, since the projected error bars from *Planck* are too large to differentiate between small and large Δ_z models.

An assumption of Equation (6) is that τ is uniform in all directions; however, reionization is naturally inhomogeneous. The optical depth will vary as function of position on the sky, which we define by the direction normal unit vector, $\hat{\mathbf{n}}$. Previously, there was an upper limit constraint put on the rms fluctuation in τ of, at most, a few percent of the mean value

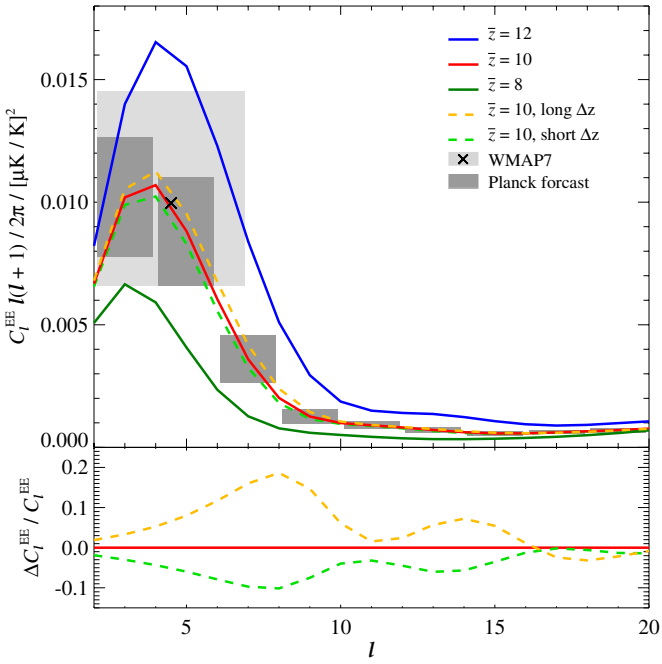

Figure 2. Top: the low-ℓ *EE* polarization power spectrum for several models of reionization compared to the *WMAP* seven year band power constraint (light gray box; Larson et al. 2011) and the projected error bars from *Planck* (dark gray bands; The Planck Collaboration 2006) for the 143 GHz channel calculated for our fiducial model. We show five models: our fiducial model at $\bar{z} = 8$, 10, and 12 (green, red, and blue, respectively) and two extreme models of short- (orange dashed) and long- (light green dashed) duration reionization at a fixed $\bar{z} = 10$. Bottom: the fractional difference between our fiducial and the two extreme models. The low-ℓ *EE* polarization power spectrum will tightly constrain $\bar{z}$. However, it is not possible to discern between our models with large or small Δ_z for same $\bar{z}$ using only this measurement.

(A color version of this figure is available in the online journal.)

$\langle\tau\rangle$ using published SPT data (Mortonson & Hu 2010). Given this upper limit, the patchy τ contribution to the CMB power spectrum at high ℓ is negligible. In Paper II, we show that four-point statistics of the CMB, in principle, can constrain the rms fluctuation in τ and, if measured, one can differentiate between models with small and large Δ_z and possibly break this degeneracy between Δ_z and $\bar{z}$. This approach differs from other approaches to measure patchy τ (e.g., Dvorkin & Smith 2009; Su et al. 2011) because it uses a four-point estimator in the

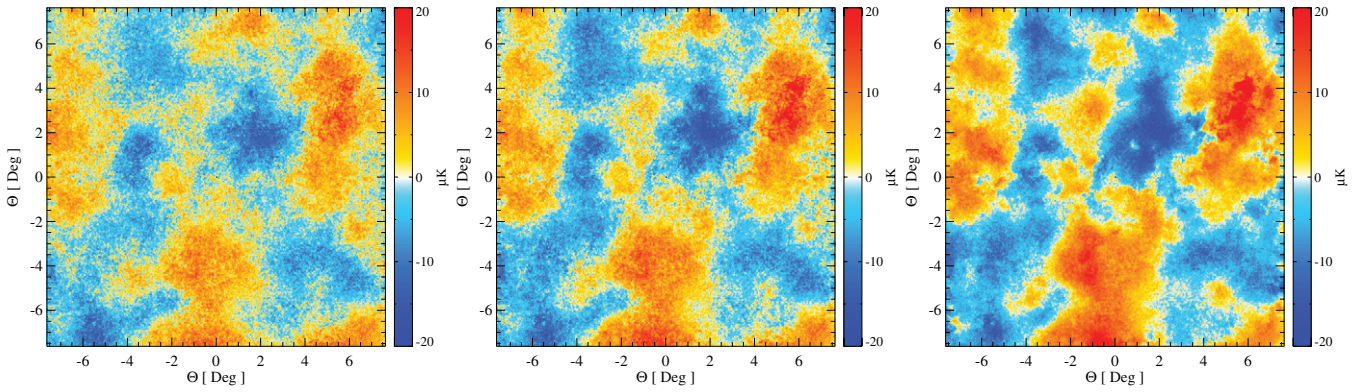

Figure 3. Light cone projected maps of the kSZ signal from patchy reionization for models with $\bar{z} = 10$ and our largest (left), fiducial (center), and smallest Δ_z (right). The overall large-scale structure is similar but the small-scale structure decreases as Δ_z decreases.

(A color version of this figure is available in the online journal.)

coincidence limit instead of quadratic estimators (see Paper II for more details).

3.2. Patchy Kinetic Sunyaev–Zel'dovich Power Spectrum

The kSZ signal from patchy reionization is sensitive to the details of reionization such as the mean redshift of reionization and its duration (e.g., McQuinn et al. 2005; Zahn et al. 2005, 2012; Mesinger et al. 2012). The physical explanation for this sensitivity is that the average proper density of the universe increases with redshift and the number of ionized bubbles traversed depends on the duration. In this section, we investigate how the patchy kSZ power spectrum depends on our model parameters and we compare our results against previous work and observational constraints. We provide a simple scaling relation for the patchy kSZ power at $\ell = 3000$ as a function of $\bar{z}$ and Δ_z, which makes model fitting of observational spectra trivial.

We construct patchy kSZ maps by ray tracing through the past light cone from $z = 5.5$ to $z = 20$, which defines the redshift range we consider for the patchy kSZ component. The temperature distortion along each line of sight is given by

$$\frac{\Delta T}{T}(\hat{\mathbf{n}}) = \frac{\sigma_{\rm T}}{c} \int_{l_{\rm o}}^{l} e^{-\tau(l,\hat{\mathbf{n}})} n_{\rm e}(l, \hat{\mathbf{n}}) \hat{\mathbf{n}} \cdot \mathbf{v} dl, \quad (7)$$

where $\mathbf{v}$ is the peculiar velocity, $\tau(\hat{\mathbf{n}})$ is from Equation (6) including the directional dependence, and $l_{\rm o}$ is the proper distance at $z = 5.5$. When constructing these light cones, we use linear theory to evolve the density between the outputs of the N-body simulations, but the velocity fields remain unaltered at the output value. We make flat-sky maps that are approximately $15^\circ \times 15^\circ$, where this angular size is determined by the N-body simulation box length of 2 Gpc h^{-1} over the comoving distance out to $z = 20$. Since the box length ($L = 2$ Gpc h^{-1}) of the N-body simulations is approximately equal to the comoving distance between $z = 6$ and $z = 20$, we cycle through the projection direction coordinates approximately once when making the maps. For each choice of parameters, we make three maps along three independent axes. In Figure 3 we show the patchy kSZ Compton-y maps for our fiducial model and the two extreme models for the same projection direction. From these maps it is obvious how the duration of ionization affects the patchy kSZ. The models of reionization with large Δ_z have more small-scale structure than models with small Δ_z.

Using the flat-sky approximation we calculate the power spectrum from the patchy kSZ maps and average over each projection axis for a given parameterization. Figure 4 shows the patchy kSZ power spectrum for various models of reionization from the $15^\circ \times 15^\circ$ patches. We find that increasing $\bar{z}$ with a fixed Δ_z increases the overall amplitude of the patchy kSZ power spectrum, but has little effect on the shape. This dependence comes from changing the integration path lengths since we defined the patchy kSZ component to come from $z > 5.5$. For example, a model with a high $\bar{z}$ will receive contributions to power from a larger fully ionized region than a lower $\bar{z}$ model. Altering Δ_z at fixed $\bar{z}$ changes both the amplitude and shape of the patchy kSZ power spectrum since Δ_z affects the correlation between ionized regions (Paper I) and the path length that CMB photons will travel through ionized regions. Specific to our model, we find the trend that parameters that produce smaller Δ_z values have large ionized regions and more power at smaller ℓ. Conversely, parameters that produce larger Δ_z values have more power at larger ℓ due to the smaller

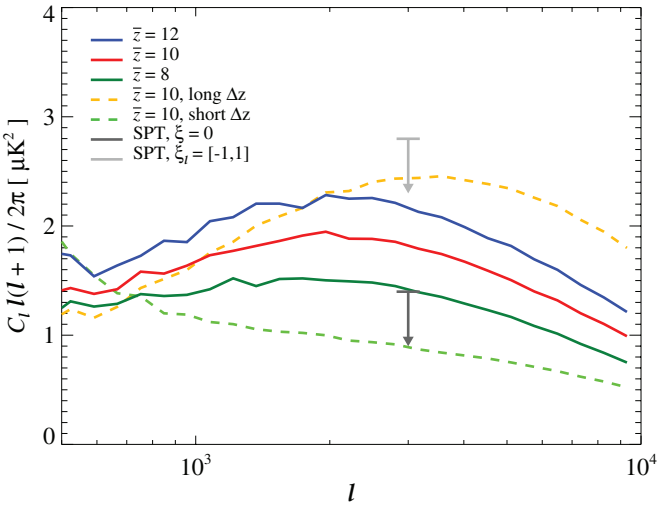

Figure 4. Patchy kSZ power spectrum for various reionization models compared to SPT constraints (Zahn et al. 2012). We show five models: our fiducial model at $\bar{z} = 8$, 10, and 12 (green, red, and blue, respectively) and two extreme models of long- (orange dashed) and short- (light green dashed) duration reionization at a fixed $\bar{z} = 10$. The SPT constraints are illustrated by the gray arrows, with the darker gray arrow representing the constraint ignoring the tSZ–CIB cross-correlation and light including this correlation. All our of models fall below the constraint that allows for tSZ–CIB correlation with an ℓ-dependent shape. Only the short-duration model is below the tighter constraint from SPT, which ignores this correlation.

(A color version of this figure is available in the online journal.)

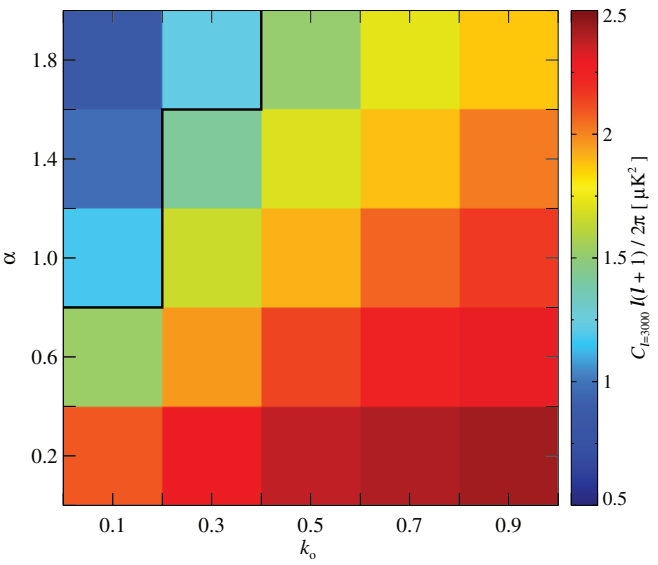

Figure 5. Parameter study of the patchy kSZ power spectrum at $\ell = 3000$ for varying k_o and α with a fixed $\bar{z} = 10$. The black line indicates the upper limit from SPT (Zahn et al. 2012) with $\xi = 0$ and all models above that are consistent with this constraint. The bottom right corner has the largest Δ_z and the top left corner has the shortest Δ_z. A brief physical understanding of the parameters is that increasing α shortens reionization while increasing k_o prolongs it.

(A color version of this figure is available in the online journal.)

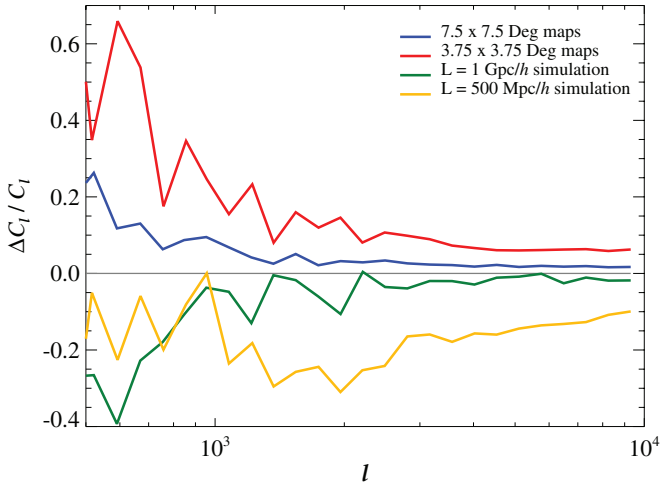

Figure 6. Fractional difference comparing the average patchy kSZ power spectra of maps constructed from smaller volume N-body simulations (green and orange lines) and cut-out maps (red and blue lines) to the original $15^\circ \times 15^\circ$ maps using the fiducial parameters with $\bar{z} = 10$. The average power spectrum of the maps constructed from the smaller volume simulations have less power than our $15^\circ \times 15^\circ$ spectrum, while the smaller cut-out maps have more power.

(A color version of this figure is available in the online journal.)

coherent ionized regions. However, it maybe possible to construct a fine-tuned model where this trend breaks. These results are qualitatively similar to Mesinger et al. (2012) and Zahn et al. (2012). The strong shape and amplitude dependencies of the patchy kSZ power spectrum on Δ_z illustrates that if there are constraints on $\bar{z}$ from the *EE* power spectrum and τ, then a measurement of the patchy kSZ power spectrum will break the degeneracy between $\bar{z}$ and Δ_z. The recent SPT results (Zahn et al. 2012) showed that the patchy kSZ power spectrum will break the degeneracy between Δ_z and the beginning and the end of reionization, which is consistent with our findings. However, we defined the patchy kSZ contribution to start from $z = 5.5$ and have not adjusted the starting redshift to match the various ionization histories from the models. Given these choices, it is natural to use $\bar{z}$ in this work instead of the beginning and end of reionization. Additionally, the beginning and end of reionization are the most uncertain epochs in both simulations and semi-analytic methods.

In Figure 4, our patchy kSZ power spectra are compared against the SPT upper limits (Zahn et al. 2012), which were recalculated to be consistent with our patchy kSZ definition. We calculated these modified upper limits by taking the total kSZ upper limits from SPT and then subtracting the homogenous kSZ contribution ($z < 5.5$) using the model from Shaw et al. (2012). Here the tightest constraint from SPT does not account for any correlation, ξ, between thermal SZ and the cosmic infrared background (CIB), which was measured at $\ell = 3000$ to be $\xi_{\ell=3000} = -0.18 \pm 0.2$ (Reichardt et al. 2012). The other two constraints account for a non-zero ξ, where ξ is given a uniform prior from -1 to 1 and either includes an ℓ-dependent shape constraint or does not. We find that our fiducial model is consistent with SPT upper limits, which includes a non-zero tSZ–CIB correlation. Figure 5 shows our parameter space study of α and k_o for the patchy kSZ power at $\ell = 3000$ with $\bar{z} = 10$. The amplitudes of the patchy kSZ power in Figure 5 range from 0.87 to 2.42 μK^2 and most models with large Δ_z (i.e., low α and large k_o) do not fall below the SPT constraints that exclude the tSZ–CIB correlation (cf. Figure 4). However, this does not exclude these models since ξ is expected to be non-zero.

The kSZ power spectra that our model produces are lower than earlier predictions from both semi-analytic models and simulations (e.g., McQuinn et al. 2005; Zahn et al. 2005; Iliev et al. 2007). Part of this discrepancy results from using different cosmological parameters. More recent predictions from Zahn et al. (2012) and Mesinger et al. (2012) are consistent with this work and similar trends are found between the different parameters of the models that govern Δ_z. For example, when we increase α the kSZ power spectrum is affected in a similar way to an increase in the parameters that govern the ionization efficiency or the minimum virial temperature of ionizing halos (Mesinger et al. 2012).

The earlier works used smaller maps constructed from smaller volume simulations to calculate the patchy kSZ signal (e.g., Zahn et al. 2005; Iliev et al. 2007), whereas we calculated the patchy kSZ on $15^\circ \times 15^\circ$ maps constructed from an N-body simulation with a box length of 2 Gpc h^{-1}. These maps contain large velocity structures (cf. Figure 3) that would not be captured by smaller volume simulations or smaller maps. Thus, using smaller maps or smaller volume simulations to construct maps cause biases in the kSZ power spectrum. We checked the amount of bias that maps constructed from smaller volume simulations produced by performing the same patchy kSZ calculation on N-body simulations box with lengths of 1 Gpc h^{-1} and 500 Mpc h^{-1} (map sizes of $7.^\circ5 \times 7.^\circ5$ and $3.^\circ75 \times 3.^\circ75$, respectively). In Figure 6, we show that compared to our original kSZ power spectrum the maps from the smaller volume simulations have less power. At $\ell = 3000$ this biases are $\sim$2% and $\sim$15% for the 1 Gpc h^{-1} and 500 Mpc h^{-1} simulations, respectively. A smaller volume simulation does not contain the large-scale velocity modes of a large one. The absences of these modes causes the amplitude of the patchy kSZ to decrease and affects the homogenous kSZ the same way (e.g., Shaw et al. 2012). The amount of bias smaller maps produced was checked by dividing our original maps into 4 $7.^\circ5 \times 7.^\circ5$

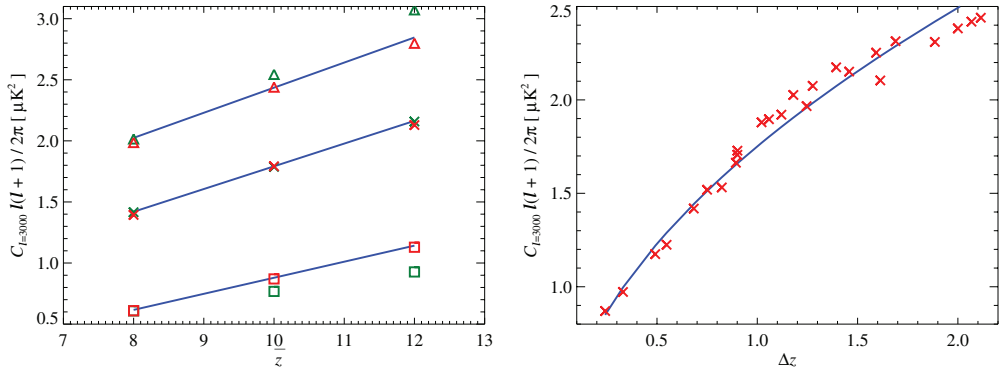

Figure 7. Scaling relations between the patchy kSZ amplitude at $\ell = 3000$ and Δ_z and $\bar{z}$. Shown are the best-fit relations (blue lines) compared to the kSZ amplitudes from the maps (red symbols). Left: the patchy kSZ amplitude at $\ell = 3000$ as a function of $\bar{z}$ scales like $D^{\rm kSZ}_{\ell=3000} \propto \bar{z}$. This scaling is compared across different reionization durations of $\Delta_z = 0.2$, 1.05, and 2.10 (squares, crosses, and triangles, respectively), and against the combined scaling law (cf. Equation (10), green symbols). Right: the patchy kSZ amplitude at $\ell = 3000$ as a function of Δ_z scales like $D^{\rm kSZ}_{\ell=3000} \propto \Delta_z^{0.5}$, here $\bar{z} = 10$. The combined scaling relation can be used to constrain the EoR in secondary parameter fitting of the high-ℓ CMB measurements.

(A color version of this figure is available in the online journal.)

and 16 3.°75 × 3.°75 cut-out maps (totaling 12 and 48 maps, respectively). We calculate the spectra for each new smaller map and average them together. The average power spectrum of the small maps had more power (cf. Figure 6). Compared to the original power spectrum, the biases at $\ell = 3000$ are ∼2% and ∼10% for the 7.°5 × 7.°5 maps and 3.°75 × 3.°75 maps, respectively. Small ıcut-out maps are susceptible to erroneously producing more power on scales of interest because of two major reasons. (1) Large-scale features may be artificially truncated at the boundaries of the non-periodic maps. (2) The subsample of kSZ values may not be representative of the entire distribution, and therefore both the mean and variance will deviate from their proper values. The competing biases mentioned above could conspire to cancel out, but in general they will not.

We found that the dependence of the amplitude of the patchy kSZ power spectrum at $\ell = 3000$ on $\bar{z}$ and Δ_z can be represented by simple scaling laws. Figure 7 illustrates these dependencies of $D^{\rm kSZ}_{\ell=3000} \equiv C^{\rm kSZ}_{\ell=3000}\ell(\ell+1)/(2\pi)$, which is linear for $\bar{z}$ and a power law for Δ_z. When fitting for the scaling laws, we use a nonlinear least-squares method where each value is weighted by the inverse of the variance of the three different projections and treat the dependence of $D^{\rm kSZ}_{\ell=3000}$ on $\bar{z}$ and Δ_z as separable functions. The scaling laws are constrained to be

$$D^{\rm kSZ}_{\ell=3000} = 1.78\ \mu{\rm K}^2 \left[1.14\left(\frac{1+\bar{z}}{11}\right) - 0.14\right] \qquad (8)$$

for a fixed $\Delta_z = 1.05$ and

$$D^{\rm kSZ}_{\ell=3000} = 1.78\ \mu{\rm K}^2 \left(\frac{\Delta_z}{1.05}\right)^{0.51} \qquad (9)$$

for a fixed $\bar{z} = 10$. The combination of Equations (8) and (9) gives

$$D^{\rm kSZ}_{\ell=3000} \simeq 2.03\ \mu{\rm K}^2 \left[\left(\frac{1+\bar{z}}{11}\right) - 0.12\right]\left(\frac{\Delta_z}{1.05}\right)^{0.51}. \qquad (10)$$

The predicted $D^{\rm kSZ}_{\ell=3000}$ from Equation (10) compares well to the results from our model (cf. Figure 7). Small deviations are seen in the variation of the map power spectrum values about the fit (right panel, Figure 7) and these deviations are found at the extreme ends of parameter space. Note that this scaling relation is specific to our definition of the patchy kSZ contribution. If there are significant contributions to reionization from more exotic physics that produce large asymmetries in x_i, this scaling relation does not hold (Park et al. 2013). In such cases, it is perhaps better to scale with the optical depth instead of $\bar{z}$. Using Equation (10) we find a lower limit of $D^{\rm kSZ}_{\ell=3000} \gtrsim 0.4\ \mu{\rm K}^2$ by taking the 2σ lower confidence interval on $\bar{z} = 8.1$ from *WAMP7* and the lower limit on $\Delta_z \gtrsim 0.07$ from EDGES. Here we converted the EDGES definition of Δ_z, which assumes a functional form of hyperbolic tangent for $x_i(z)$ to our definition. This scaling law provides a simple way to place model-dependent constraints on $\bar{z}$ or Δ_z by including it when fitting high-ℓ CMB power spectra measurements into the secondary models used. However, this requires additional measurements, for example, of the *EE* power spectrum, to break the degeneracies between Δ_z and $\bar{z}$ that occurs when just using patchy kSZ measurements.

4. FUTURE CONSTRAINTS

Constraints on $\bar{z}$ and Δ_z will tighten as the precision increases on measurements of the low-ℓ *EE* polarization and high-ℓ temperature power spectra. We forecast how well these future precision measurements of τ and $D_{\ell=3000}$ will constrain $\bar{z}$ and Δ_z by constructing a likelihood surface from a χ^2 grid of $\bar{z}$ and Δ_z around our fiducial model. The χ^2 grid is calculated following

$$\chi^2 = \left[\frac{\tau - \tau_{\rm fid}}{\sigma_\tau}\right]^2 + \left[\frac{D_{\ell=3000} - D_{\ell=3000,{\rm fid}}}{\sigma_{D_{\ell=3000}}}\right]^2; \qquad (11)$$

here $\tau_{\rm fid}$ and $D_{\ell=3000,{\rm fid}}$ are the values for τ and $D_{\ell=3000}$ from the fiducial model, σ_τ is the forecasted error bar for *Planck* or CMBpol on τ, and $\sigma_{D_{\ell=3000}}$ is the hypothetical error bar for ACT-pol and SPT-pol on $D_{\ell=3000}$. Using our fiducial value for τ we estimate that *Planck* will measure it to ±0.004 (∼5% error; The Planck Collaboration 2006) and CMBpol will measure it to ±0.002 (∼2.5% error; Zaldarriaga et al. 2008). There is still no detection of the patchy kSZ power spectrum, only upper limits (Reichardt et al. 2012; Zahn et al. 2012). A detection of the patchy kSZ power spectrum will depend upon the ability to properly model contributions from the thermal SZ power spectrum (which depends on uncertain intracluster medium astrophysics, e.g., Battaglia et al. 2010, 2012; Shaw et al. 2010; Trac et al. 2011), the homogeneous kSZ (e.g., Ostriker &

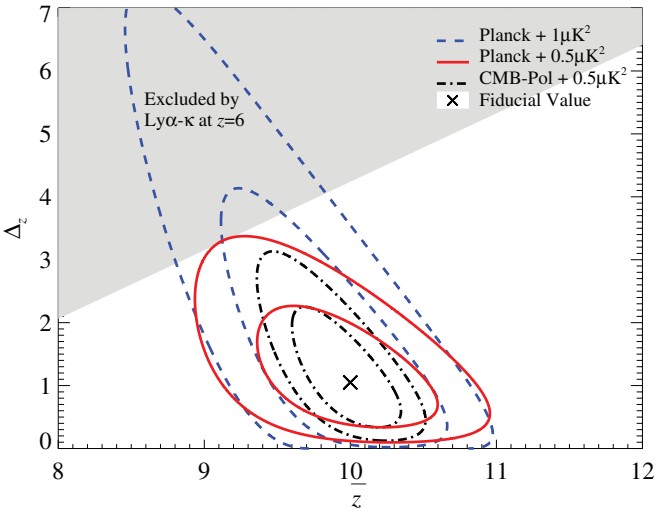

Figure 8. Projected constraints on $\bar{z}$ and Δ_z for our fiducial model of the EoR given the estimated error bars for *Planck* and CMBpol, and optimistic hypothetical error bars for ACT-pol and SPT-pol. The 1σ (inner ellipses) and 2σ (outer ellipses) constraints for *Planck* projected error bars on τ with 1 μK^2 (blue dashed lines) and 0.5 μK^2 (red lines) estimated error bars for ACT-pol and SPT-pol on $D_{\ell=3000}$ patchy kSZ measurements. The black dot-dashed lines are the 1σ and 2σ constraints for CMBpol projected error bars on τ and 0.5 μK^2 estimated error bars for ACT-pol and SPT-pol on $D_{\ell=3000}$ patchy kSZ measurements. The gray region across the top is excluded by the zero transmission of rest-frame Lyα flux at $z \gtrsim 6$ in spectra of quasars (Lyα-κ; Fan et al. 2006b).

(A color version of this figure is available in the online journal.)

Vishniac 1986; Jaffe & Kamionkowski 1998; Ma & Fry 2002; Zhang et al. 2004; Shaw et al. 2012), the thermal SZ–CIB cross spectrum (Reichardt et al. 2012; Addison et al. 2012; Zahn et al. 2012), and the infrared and radio sources (see Dunkley et al. 2011; Reichardt et al. 2012 for these models). We choose two hypothetical error bar values for ACT-pol and SPT-pol measurements of $D_{\ell=3000}$.

The likelihood surface is $\mathcal{L} \propto e^{-\chi^2/2}$ and the 1σ and 2σ contours are the 68% and 95% probability surface. Figure 8 show the forecasted constraints on $\bar{z}$ and Δ_z from future measurements. Results from *Planck* and a detection of the patchy kSZ power at $\ell = 3000$ will constrain $\bar{z}$ to ~5%. The value of Δ_z begins to be constrained when we combine the upper limit from the opacity of the Lyα forest (Lyα-κ) at $z = 6$ in quasar spectra. Here the upper limit from the opacity of the Lyα forest is derived by converting our Δ_z to $z(x_i = 50\%) - z(x_i = 90\%)$. Figure 8 illustrates that an experiment like CMBpol will tighten these constraints tremendously. While we focused our analysis on τ and $D_{\ell=3000}$, it is possible that the low-ℓ *EE* power spectrum from CMBpol could provide constraints on Δ_z as well, which would make our forecasted constraints even better.

5. CONCLUSIONS

Using a new semi-analytic model for constructing the reionization redshift field from any density field, we made predictions for the low-ℓ polarization power spectrum and the high-ℓ temperature spectrum measurements of the CMB. We demonstrated that combining measurements of the *EE* power spectrum with the patchy kSZ amplitude at $\ell = 3000$ constrains both the mean reionization redshift and the duration of reionization. The measured *EE* power spectrum from *WMAP* and the predicted improved spectrum from *Planck* will constrain $\bar{z}$, but cannot discern between models for reionization with extreme durations.

The shape and the amplitude of the patchy kSZ power spectrum depend on both the duration and the mean redshift of reionization. At $\ell = 3000$, where the amplitude of the kSZ power spectrum is currently constrained, we find that the patchy kSZ power in this model ranges from 0.87 to 2.42 μK^2 with $\bar{z} = 10$ (this $\bar{z}$ matches the current *WMAP* seven year constraints). The largest kSZ signals correspond to long-duration reionization models. We found a simple scaling law for the patchy kSZ power spectrum amplitude at $\ell = 3000$ as a function of $\bar{z}$ and Δ_z, which makes model fitting to observed spectra trivial. Using this scaling law and constraints from *WMAP* on the $\bar{z}$ and the lower limit from EDGES, we place a lower limit on the patchy kSZ amplitude at $\ell = 3000$ of ~0.4 μK^2.

The amplitudes we find for the patchy kSZ power spectra are lower than previous model predictions. Besides the different cosmological parameters, the differences between our work and the earlier work on the patchy kSZ signal (Zahn et al. 2005; Iliev et al. 2007) are that previous work used much smaller maps from constructed from smaller simulation volumes to calculate this signal. We show that patchy kSZ power spectra are biased low when maps from smaller volume simulations are used. Additionally, this signal is biased high when smaller maps are used.

Many of our reionization models are consistent with the upper limit constraint from SPT that accounts for correlations between the tSZ and CIB (Zahn et al. 2012). One of these models is our fiducial one, which has $\bar{z} = 10$ and $\tau = 0.085$ and is consistent with the current *WMAP* seven year constraints. This consistency is achieved without the need to invoke more exotic or unphysical models for reionization that were necessary for the previous models of the patchy kSZ in order to fit these constraints. In the event that the measured values of τ and $\bar{z}$ decrease, the patchy kSZ power for all models would decrease further.

It is clear that the future measurements from the *Planck* satellite of the *EE* power spectrum will tightly constrain the mean reionization redshift and CMBpol has the potential to do even better. This leaves measurements of the patchy kSZ power spectrum from high-resolution CMB observations to constrain the duration of the EoR. The current upper limits of the patchy kSZ amplitude at $\ell = 3000$ reported by SPT range from 2.1 to 4.9 μK^2 depending on the assumptions made about the correlation between the tSZ and CIB, but future detections are projected to be ~1 μK^2 (Reichardt et al. 2012). In order to measure the patchy kSZ, we first need to understand ξ (Reichardt et al. 2012; Addison et al. 2012; Zahn et al. 2012), have a good understanding of the contributions from the homogenous kSZ (e.g., Ostriker & Vishniac 1986; Jaffe & Kamionkowski 1998; Ma & Fry 2002; Zhang et al. 2004; Shaw et al. 2012), and the astrophysical uncertainties associated with the homogenous kSZ. A measurement of the patchy kSZ will tighten the constraints on Δ_z greatly.

Combining these CMB constraints with neutral hydrogen measurements (e.g., P. La Plante et al. 2013, in preparation), such as redshifted 21 cm signal that originates from the hyperfine transition of neutral hydrogen (e.g., Scott & Rees 1990; Shaver et al. 1999; Zaldarriaga et al. 2004), will constrain the mean redshift and duration of reionization further or provide new issues for reionization models to tackle.

N.B. and A.N. are supported by a McWilliams Center for Cosmology Postdoctoral Fellowship made possible by Bruce and Astrid McWilliams Center for Cosmology. We thank Graeme

Addison, Gil Holder, Eiichiro Komatsu, Andrei Mesinger, Paul La Plante, Christian Reichardt, Jonathan Sievers, and Oliver Zahn for useful discussions. H.T. is supported in part by NSF grant AST-1109730. R.C. is supported in part by NSF grant AST-1108700 and NASA grant NNX12AF91G. A.L. is supported in part by NSF grant AST-0907890 and NASA grants NNX08AL43G and NNA09DB30A. The simulations were performed at the Pittsburgh Supercomputing Center (PSC) and the Princeton Institute for Computational Science and Engineering (PICSciE). We thank Roberto Gomez and Rick Costa at the PSC and Bill Wichser at PICSciE for invaluable help with computing.

REFERENCES

Addison, G. E., Dunkley, J., & Spergel, D. N. 2012, MNRAS, 427, 1741
Barkana, R., & Loeb, A. 2004, ApJ, 609, 474
Battaglia, N., Bond, J. R., Pfrommer, C., & Sievers, J. L. 2012, ApJ, 758, 75
Battaglia, N., Bond, J. R., Pfrommer, C., Sievers, J. L., & Sijacki, D. 2010, ApJ, 725, 91
Battaglia, N., Trac, H., Cen, R., & Loeb, A. 2013, ApJ, in press
Bolton, J. S., Haehnelt, M. G., Warren, S. J., et al. 2011, MNRAS, 416, L70
Bond, J. R., & Efstathiou, G. 1987, MNRAS, 226, 655
Bowman, J. D., & Rogers, A. E. E. 2012, arXiv:1209.1117
Dunkley, J., Hlozek, R., Sievers, J., et al. 2011, ApJ, 739, 52
Dvorkin, C., & Smith, K. M. 2009, PhRvD, 79, 043003
Fan, X., Carilli, C. L., & Keating, B. 2006a, ARA&A, 44, 415
Fan, X., Strauss, M. A., Becker, R. H., et al. 2006b, AJ, 132, 117
Gruzinov, A., & Hu, W. 1998, ApJ, 508, 435
Haiman, Z., & Cen, R. 2005, ApJ, 623, 627
Hu, W., & White, M. 1997, PhRvD, 56, 596
Iliev, I. T., Pen, U.-L., Bond, J. R., Mellema, G., & Shapiro, P. R. 2007, ApJ, 660, 933
Jaffe, A. H., & Kamionkowski, M. 1998, PhRvD, 58, 043001
Jelić, V., Zaroubi, S., Aghanim, N., et al. 2010, MNRAS, 402, 2279
Knox, L., Scoccimarro, R., & Dodelson, S. 1998, PhRvL, 81, 2004
Komatsu, E., Smith, K. M., Dunkley, J., et al. 2011, ApJS, 192, 18
Larson, D., Dunkley, J., Hinshaw, G., et al. 2011, ApJS, 192, 16
Lewis, A., Challinor, A., & Lasenby, A. 2000, ApJ, 538, 473
Liu, G.-C., Sugiyama, N., Benson, A. J., Lacey, C. G., & Nusser, A. 2001, ApJ, 561, 504
Ma, C.-P., & Fry, J. N. 2002, PhRvL, 88, 211301
Malhotra, S., & Rhoads, J. E. 2004, ApJL, 617, L5
McQuinn, M., Furlanetto, S. R., Hernquist, L., Zahn, O., & Zaldarriaga, M. 2005, ApJ, 630, 643
McQuinn, M., Lidz, A., Zaldarriaga, M., Hernquist, L., & Dutta, S. 2008, MNRAS, 388, 1101
Mesinger, A., Furlanetto, S., & Cen, R. 2011, MNRAS, 411, 955
Mesinger, A., & Furlanetto, S. R. 2008, MNRAS, 385, 1348
Mesinger, A., & Haiman, Z. 2004, ApJL, 611, L69
Mesinger, A., McQuinn, M., & Spergel, D. N. 2012, MNRAS, 422, 1403
Mortonson, M. J., & Hu, W. 2008, ApJ, 672, 737
Mortonson, M. J., & Hu, W. 2010, PhRvD, 81, 067302
Natarajan, A., Battaglia, N., Trac, H., Li Pen, U., & Loeb, A. 2013, ApJ, in press
Ostriker, J. P., & Vishniac, E. T. 1986, ApJL, 306, L51
Park, H., Shapiro, P. R., Komatsu, E., et al. 2013, ApJ, 769, 93
Reichardt, C. L., Shaw, L., Zahn, O., et al. 2012, ApJ, 755, 70
Santos, M. G., Cooray, A., Haiman, Z., Knox, L., & Ma, C.-P. 2003, ApJ, 598, 756
Scott, D., & Rees, M. J. 1990, MNRAS, 247, 510
Shaver, P. A., Windhorst, R. A., Madau, P., & de Bruyn, A. G. 1999, A&A, 345, 380
Shaw, L. D., Nagai, D., Bhattacharya, S., & Lau, E. T. 2010, ApJ, 725, 1452
Shaw, L. D., Rudd, D. H., & Nagai, D. 2012, ApJ, 756, 15
Su, M., Yadav, A. P. S., McQuinn, M., Yoo, J., & Zaldarriaga, M. 2011, arXiv:1106.4313
Sunyaev, R. A., & Zeldovich, I. B. 1980, MNRAS, 190, 413
The Planck Collaboration 2006, arXiv:0604069
Totani, T., Kawai, N., Kosugi, G., et al. 2006, PASJ, 58, 485
Trac, H., Bode, P., & Ostriker, J. P. 2011, ApJ, 727, 94
Trac, H., Cen, R., & Loeb, A. 2008, ApJL, 689, L81
Valageas, P., Balbi, A., & Silk, J. 2001, A&A, 367, 1
Wyithe, J. S. B., Loeb, A., & Carilli, C. 2005, ApJ, 628, 575
Zahn, O., Reichardt, C. L., Shaw, L., et al. 2012, ApJ, 756, 65
Zahn, O., Zaldarriaga, M., Hernquist, L., & McQuinn, M. 2005, ApJ, 630, 657
Zaldarriaga, M. 1997, PhRvD, 55, 1822
Zaldarriaga, M., Colombo, L., Komatsu, E., et al. 2008, arXiv:0811.3918
Zaldarriaga, M., Furlanetto, S. R., & Hernquist, L. 2004, ApJ, 608, 622
Zhang, P., Pen, U.-L., & Trac, H. 2004, MNRAS, 347, 1224